Proceedings of the
Annual Stability Conference
Structural Stability Research Council
Atlanta, Georgia, April 21-24, 2026

Buckling behavior of laced built-up steel columns considering local/global/built-up interaction

Oudom Chhoeng[1], Morane Chloé Mefande Wack[2], Robert Tremblay[3], Nicolas Boissonnade[4]

Abstract

This study investigates the stability behavior of laced built-up steel columns that buckle in the plane of the lacing system, where shear deformation plays a critical role in reducing axial capacity. The columns are composed of C-shaped chords connected by double (X) flat lacing bars, and exhibit a complex interaction of local, global, and built-up (L/G/B) buckling modes. Three principal instability modes are examined: (i) local buckling of cross-sections, (ii) global buckling of individual chords between lacing points, and (iii) built-up buckling of the overall member. For slender members, current design provisions in Eurocode 3 and AISC fail to capture these interactions accurately, often leading to unconservative strength predictions. To address these shortcomings, this work extends the Overall Interaction Concept (O.I.C.), previously applied to local/global interactions, to explicitly incorporate the built-up buckling mechanism. The proposed approach is calibrated using validated shell finite element models, and its effectiveness is demonstrated through a comprehensive parametric study. Comparison with existing design methods shows that the extended O.I.C. offers more accurate, consistent, and safer strength predictions for both tip-to-tip and back-to-back configurations. Statistical verification is performed in accordance with EN 1990, further supporting the method's reliability for use in design.

1. Introduction

This paper focuses on the design of laced built-up columns subjected to axial compression, specifically those that buckle within the plane of the lacing system. These types of members were frequently used in truss bridge design during the late 19th and early 20th centuries. Due to the limitations of steel manufacturing and fabrication techniques at the time, engineers combined smaller components like plates, angles, and channels to create larger, stronger structural elements. This method was cost-effective, optimized material usage and made transportation and assembly of large bridge components easier. While these designs provided benefits such as increased bending stiffness, they also introduced challenges, such as shear flexibility, which compromised buckling resistance. Today, steel built-up members like those used in early truss bridges are rarely

[1] PhD, Polytechnique Montréal, <oudom.chhoeng@polymtl.ca>
[2] PhD, Polytechnique Montréal, <morane-chloe.mefande-wack@polymtl.ca>
[3] Professor, Polytechnique Montréal, <robert.tremblay@polymtl.ca>
[4] Professor, Université Laval, <nicolas.boissonnade@gci.ulaval.ca>

seen, as they have been largely replaced by heavy structural sections from rolling mills or welded shapes produced by steel manufacturers. Despite this, many of these older bridges remain in use, with components that often do not conform to modern design codes. This creates difficulties in assessing the structural integrity of the built-up members in these existing truss bridges, a concern underscored by historical failures such as the collapse of the Quebec Bridge, which tragically highlighted the consequences of inadequate understanding of built-up member buckling.

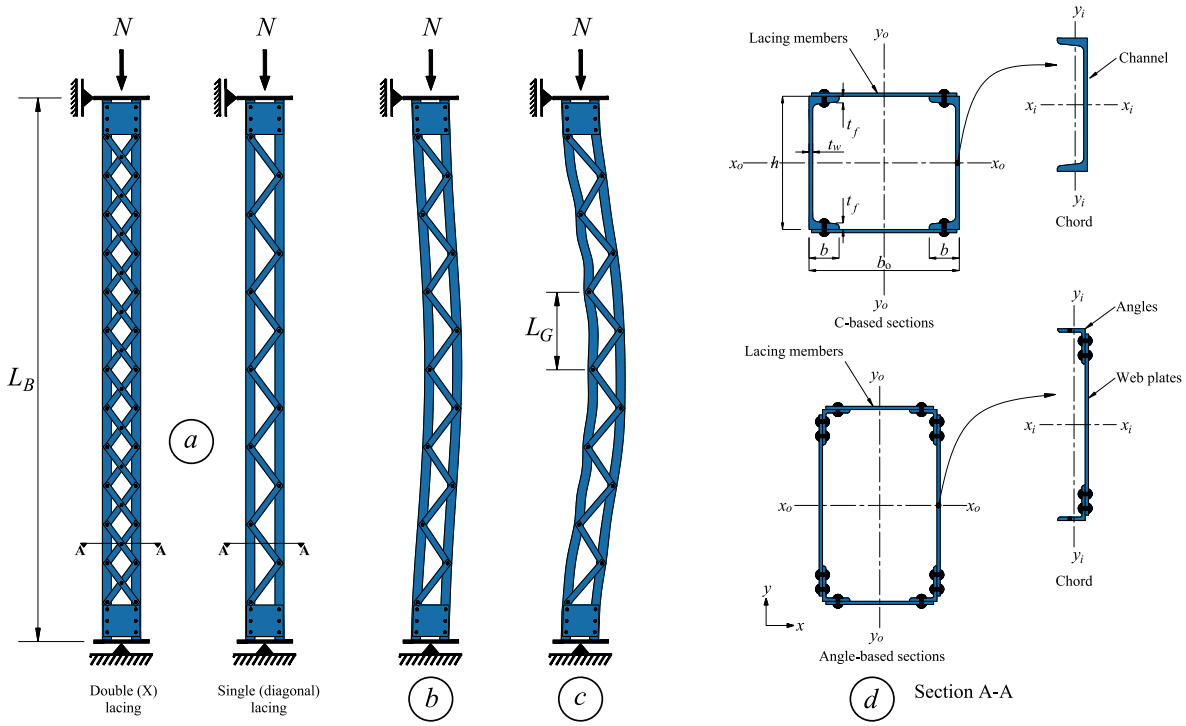

Figure 1: Buckling of a built-up member involving shear deformation

Following the first collapse of built-up members in the Quebec Bridge, the impact of shear deformations on the buckling capacity of built-up sections became a significant concern (Galbraith & Holgate Derry, 1908). This issue was investigated by numerous researchers. To clearly illustrate the buckling behavior of built-up members, Figure 1 presents various configurations: Figure 1a shows a typical built-up member under axial compression, Figure 1b depicts buckling under flexure and Figure 1c shows buckling involving both flexure and shear deformations. As shown in Figure 1c, when buckling occurs about the y_o axis of the section (buckling in-plane of lacing system), the members may deform due to a combination of flexural and shear effects. In this scenario, flexural deformations arise from the overall global buckling of the built-up member (built-up buckling), while the shear deformations result from the global flexural buckling of the individual chords between the lacings (global buckling) around their minor-axis of bending. These additional shear deformations lead to a reduction in the member's buckling load. This issue was first investigated by (Engesser, 1891) and later by Timoshenko (1930), who proposed an equation for the elastic buckling critical load of pinned members. Timoshenko's formulation accounted for the combined effects of built-up flexural buckling and global buckling of individual chords between connectors due to shear. These classical equations are documented in standard stability textbooks (Timoshenko & Gere, 1961; Bleich, 1952). Building on this work, Aslani and Goel (1991) extended the formulation to general boundary conditions and introduced a theory-based

modified slenderness ratio for built-up members. This approach was subsequently adopted by most design codes, which treat Built-up (B) buckling and Global (G) buckling of chords between connectors independently, without explicitly accounting for their interaction, commonly referred to as Global/Built-up (G/B) interaction. The interaction between built-up buckling of the overall member and global buckling of individual chords was examined by Svensson and Kragerup (1982), Geng-Shu and Shao-Fan (1989), Duan et al. (2002), and more recently by Li et al. (2019). These studies primarily focused on the combined effects of geometric imperfections in the overall member and individual chords, rather than directly addressing the G/B interaction governing member strength. Nevertheless, their results show that such combined imperfections can significantly reduce the resistance of built-up members. Current design standards (AISC, 2022; AASHTO, 2020; AS 4100:2020) incorporate G/B interaction through modified slenderness ratios; however, the interaction between local, global and built-up buckling is not fully addressed and is often neglected. Additional code limitations are imposed to mitigate G/B interaction, which, if not adequately controlled, can lead to a significant reduction in member resistance (Duan et al., 2002). Furthermore, Local (L) buckling of the cross-section is frequently insufficiently considered, particularly regarding Local/Global/Built-up (L/G/B) interaction. In current practice, local buckling effects are typically accounted for using the Effective Width Method (EWM) (von Kármán et al., 1932), in which an effective cross-sectional area is combined with member buckling curves. Although widely used, the EWM has notable limitations, including its inability to capture interactions between plate elements and the need for iterative procedures (Seif & Schafer, 2010; Gardner et al., 2019; Boissonnade et al., 2017; L. Li & Boissonnade, 2022). It is also more suitable for members with large width-to-thickness ratios (Usami & Fukumoto, 1984).

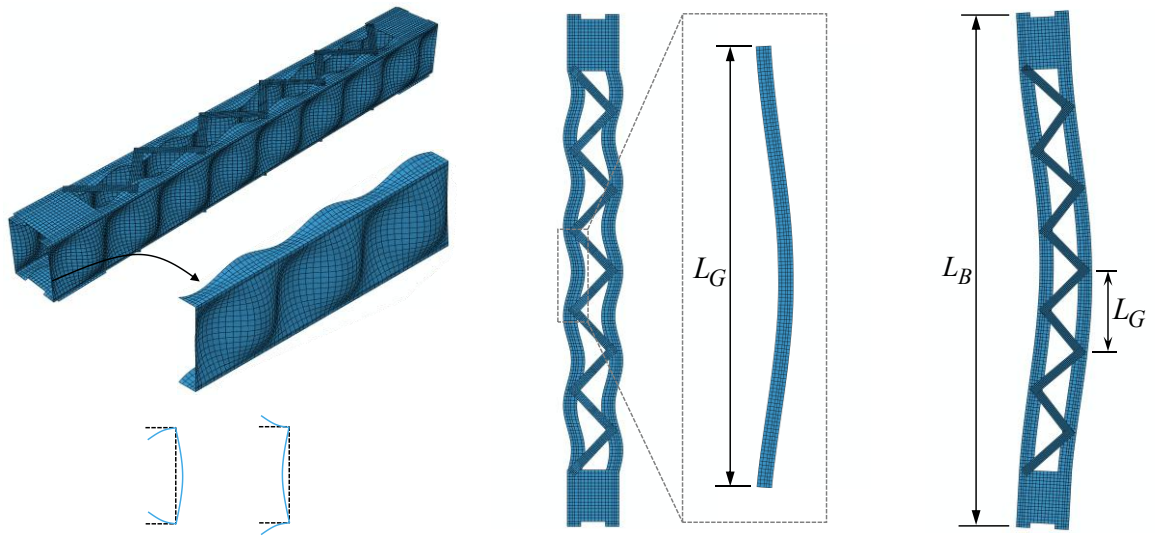

Figure 2: Buckling mode shapes of tip-to-tip laced built-up columns – (a) Local – (b) Global – (c) Built-up buckling

Overall, research addressing G/B and L/G/B interaction in built-up members remains limited, and the combined influence of local buckling, chord buckling between connectors and overall built-up buckling has not yet been thoroughly investigated. Typical buckling modes of laced built-up members are illustrated in Figure 2. Several modern design methods, including the Continuous

Strength Method (C.S.M.) (Gardner et al., 2023), the Direct Strength Method (D.S.M.) (Schafer, 2008), and the Overall Interaction Concept (O.I.C.) (Boissonnade et al., 2017), provide frameworks to account for interactive buckling in steel members. However, design approaches addressing the interaction of three buckling modes remain limited and are largely focused on cold-formed steel columns. Experimental work by (Young and Rasmussen, 1999) demonstrated a triple Local/Distortional/Global (L/D/G) interaction in cold-formed lipped channel columns, involving local cross-section buckling, distortional flange-lip buckling, and global member buckling. Subsequent studies further investigated triple interaction in cold-formed columns (Young & Yan, 2002; Dinis & Camotim, 2011; Dinis et al., 2011, 2012; Santos et al., 2012, 2014; Cava et al., 2016; Young et al., 2018; Kumar & Kalyanaraman, 2018), primarily contributing to early design concepts (Camotim et al., 2020). A comprehensive design approach was also proposed by Dinis et al. (2018), who extended the DSM to predict failure loads under L/D/G interaction. Nevertheless, DSM is inherently elastic and was developed for thin-walled cold-formed sections, limiting its applicability to stocky members governed by plastic behavior (L. Li & Boissonnade, 2022). Similarly, the CSM has mainly been applied to cold-formed stainless-steel members, where strain hardening is significant, particularly for stocky sections. The Overall Interaction Concept (OIC) was originally developed for hot-rolled sections, ranging from compact to slender members. Proposed by Boissonnade et al. (2017), it is based on clear mechanical principles and a systematic design procedure, which is briefly introduced in Section 2. Since its introduction, OIC-based approaches have been successfully extended to a wide range of hot-rolled sections, including square and hollow sections (Nseir, 2015; Michel, 2016), bi-symmetric I-sections (Gagné et al., 2020; Gérard et al., 2021; L. Li & Boissonnade, 2022; L. Li et al., 2022), mono-symmetric I-sections (L. Li et al., 2022), and T-sections (L. Li, Fafard, & Boissonnade, 2022). These studies consistently demonstrate that OIC-based design rules provide more reliable predictions than current design standards and effectively capture complex interaction effects, particularly local/global buckling. More recently, the OIC has been extended to aluminum structures (Dahboul et al., 2023; L. Li et al., 2023), where it delivers accurate, safe and economical predictions compared to existing design methods.

This paper investigates the L/G/B interactive buckling of laced built-up members under axial compression, with particular emphasis on column buckling occurring in the plane of the lacing system. The laced built-up columns consist of two hot-rolled C-sections arranged either tip-to-tip ([ ]) or back-to-back (] [), with both chords interconnected by double (X) flat lacing bars. Additionally, the lacing connectors are assumed to be riveted or bolted, and the built-up columns are subjected to axial loads under simply supported conditions. The spacing between the two C-sections ensures that the flexural buckling of the built-up section always occurs in the plane of the lacing system. The application of the O.I.C. is extended to the design of laced built-up sections that buckle in the plane of the lacing system, where a significant triple interaction mode occurs. This includes local buckling of the cross-section, global buckling of the chords between lacing connectors and built-up buckling of the overall member, all of which are examined through extensive numerical analyses.

2. O.I.C.-based design rules

2.1 O.I.C.-based design rules for double interaction

The O.I.C. is based on the well-established resistance-instability interaction, utilizing a definition of generalized relative slenderness. It eliminates the need for cross-section classification and the

E.W.M., treating all cross-section shapes uniformly at both the section and member levels. More specifically, the O.I.C. uses the plastic capacity of the section (N_{pl}) as a reference and introduces reduction (or penalty) factors (χ) to account for the detrimental effects of different buckling modes, imperfections, and their interactions.

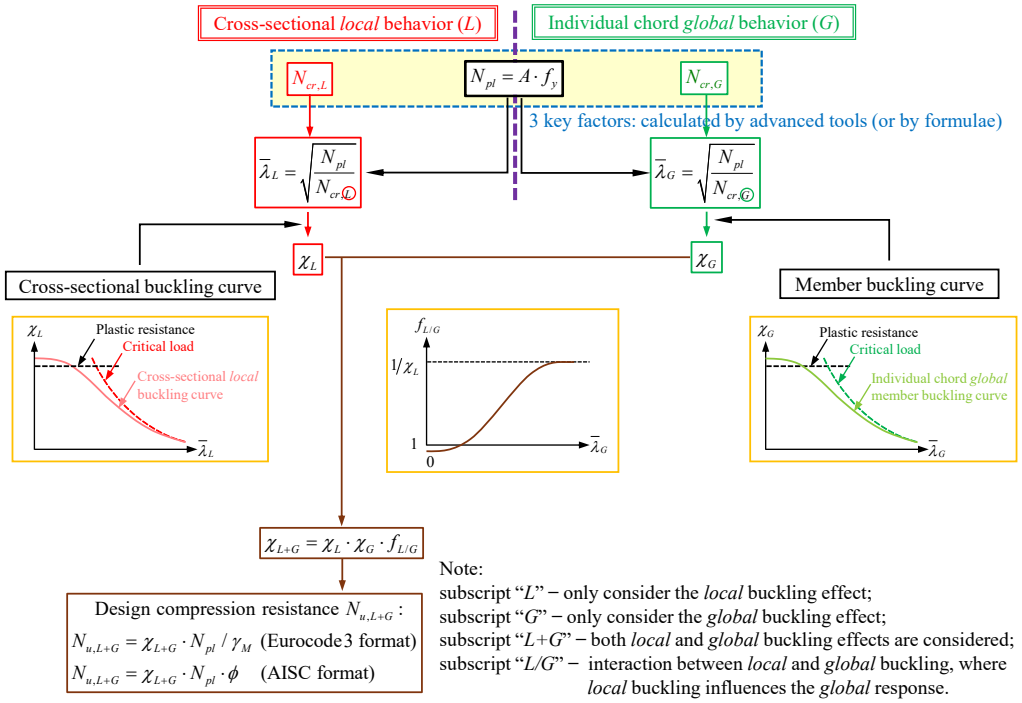

Figure 3: O.I.C. design flow chart for L/G interaction mode

Figure 3 illustrates the O.I.C. design flow chart for double *L/G* interaction modes, specifically for non-built-up members subjected to pure compression load, along with the calculation steps that need to be followed to determine the ultimate resistance. In this case, two buckling modes, i.e., local and global, have a significant effect on the capacity of members. First, the full plastic capacity (N_{pl}) of the member with the gross cross-sectional area $A_g = A$ is calculated using Eq. 1.

$$N_{pl} = A \cdot f_y \tag{1}$$

Then, the elastic local and global critical loads ($N_{cr,L}$ and $N_{cr,G}$) are determined, which represent the elastic buckling loads under local and global instability, respectively. It should be noted that these three key factors (N_{pl}, $N_{cr,L}$, and $N_{cr,G}$) are either calculated using formulas as addressed in (AISC, 2022), (American Association of State Highway and Transportation Officials, 2020), (European Committee for Standardization (CEN)), (European Committee for Standardization (CEN)) or more precisely by "advanced tools" as proposed in (Boissonnade et al., 2017). Next, the generalized local and global relative slenderness ($\bar{\lambda}_L$ and $\bar{\lambda}_G$) are defined to balance the influence of material plasticity and instability caused by geometric non-linearities. The expressions of $\bar{\lambda}_L$ and $\bar{\lambda}_G$ are given in Eq. (2).

$$\bar{\lambda}_L = \sqrt{\frac{N_{pl}}{N_{cr,L}}} \quad \text{and} \quad \bar{\lambda}_G = \sqrt{\frac{N_{pl}}{N_{cr,G}}} \tag{2}$$

Separate reduction coefficients, specifically for local buckling $\chi_L = f^o(\lambda_L)$ and global buckling $\chi_G = f^o(\lambda_G)$, are determined to account for their respective resistance-stability interactions and imperfections. Note that up to this point in the flowchart, *L* and *G* are fully independent, i.e., the *L/G* interaction has not been addressed yet. Finally, the ultimate compression resistance (N_u) is calculated by multiplying the plastic capacity (N_{pl}) by the reduction coefficients and a local/global interaction factor ($f_{L/G}$), which adjusts for the interaction between local and global effects. Therefore, when considering the effect of local/global instability, the ultimate load of a member is obtained from Eq. 3.

$$N_{u,L+G} = \chi_{L+G} \cdot N_{pl} \quad \text{where:} \quad \chi_{L+G} = \chi_L \cdot \chi_G \cdot f_{L/G} \tag{3}$$

In Eq. 3, χ_{L+G} is the penalty factor to account for the detrimental effects of local and global buckling modes (χ_L and χ_G), and their interactions ($f_{L/G}$). The O.I.C. method offers a comprehensive and unified approach to predict the behavior of different cross-section types and loading conditions while accounting for the full range of structural responses, from stocky to slender sections. Eventually, partial safety factors γ_M or ϕ may be incorporated to account for the reliability aspects of the proposed design equations, following either the European or American format, as shown in Figure 3.

2.2 Extension of O.I.C. design rules for L/G/B interaction

Following the O.I.C. concept in Figure 3, each buckling mode is addressed individually. Laced built-up members – the focus of this study – can exhibit multiple buckling behaviors, including local, global and built-up buckling, as well as interactions among them (L/G/B interactions). Accordingly, the ultimate load $N_{u,L+G+B}$ is evaluated by Eq. 4.

$$N_{u,L+G+B} = \chi_{L+G+B} \cdot N_{pl} \quad \text{where:} \quad \chi_{L+G+B} = \chi_L \cdot \chi_G \cdot \chi_B \cdot f_{L/G/B} \tag{4}$$

In Eq. 4, χ_{L+G+B} stands as an overall reduction factor accounting for the combined effects of local, global and built-up buckling. The terms χ_L , χ_G , and χ_B represent the reduction factors corresponding to the isolated (pure) local, global and built-up buckling modes, respectively, without interaction. The interaction effects among these modes are captured through the factor $f_{L/G/B}$. As discussed in Section 1, the ultimate resistance of laced built-up members may be significantly influenced by L/G/B interaction. Current design standards, such as Eurocode 3 and AISC, treat these interactions differently. Eurocode 3 addresses these effects by assuming that the strength of a built-up member is governed by the global buckling resistance of each individual chord segment between lacing connectors, while local buckling is handled through effective section properties based on section classification. In contrast, AISC treats built-up columns as a unified system, incorporating both global and built-up buckling effects into a modified slenderness ratio. Both standards handle local buckling in a similar manner through section classification and the use of the effective width method.

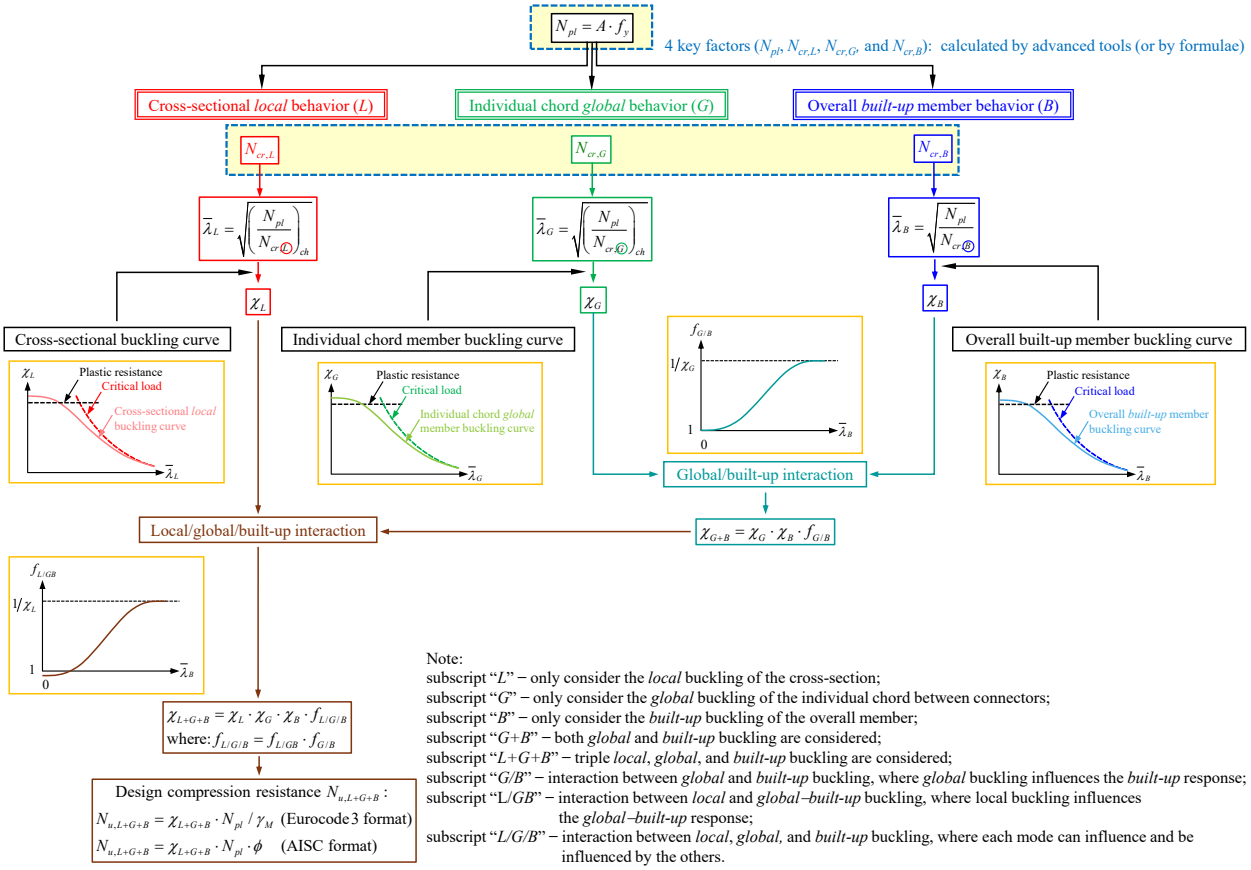

Figure 4: Proposed O.I.C. design flow chart for L/G/B interaction

Consistent with the AISC approach, this study treats the laced built-up column as a unified system by incorporating the effects of global and built-up buckling into a combined reduction factor χ_{G+B}, while addressing local buckling separately. Therefore, the interaction factor $f_{L/G/B}$ in Eq. (4) can be written in the form of Eq. (5), where correspondence with the general O.I.C. flow chart is reached through $f_{G/B} = \dfrac{\chi_{G+B}}{\chi_G \cdot \chi_B}$ and $f_{L/GB} = \dfrac{\chi_{L+G+B}}{\chi_L \cdot \chi_{G+B}}$.

$$f_{L/G/B} = f_{L/GB} \cdot f_{G/B} \tag{5}$$

In Eq. 5, $f_{G/B}$ represents the interaction between global and built-up buckling – specifically, the influence of global buckling on built-up behavior. The term $f_{L/GB}$ accounts for local interaction effects, capturing the influence of cross-sectional local buckling on the global/built-up buckling response of the member. The proposed O.I.C. design flow chart for L/G/B interaction of laced built-up columns under compression load is presented in Figure 4. In this figure, the expressions of $\bar{\lambda}_L$ and $\bar{\lambda}_G$ are formulated based on the properties of an individual chord, while $\bar{\lambda}_B$ is calculated considering the properties of the full built-up configuration.

$$\bar{\lambda}_L = \sqrt{\left(\frac{N_{pl}}{N_{cr,L}}\right)_{ch}}, \quad \bar{\lambda}_G = \sqrt{\left(\frac{N_{pl}}{N_{cr,G}}\right)_{ch}} \quad \text{and} \quad \bar{\lambda}_B = \sqrt{\frac{N_{pl}}{N_{cr,B}}} \tag{6}$$

Here, N_{pl} at the local and global levels is determined using the gross cross-sectional area of an individual chord (A_{ch}), while N_{pl} at the built-up level is calculated based on the gross cross-sectional area of the entire built-up section (A). The values of $N_{cr,G}$ and $N_{cr,B}$ are defined by Eq. 7, where I_{ch} and I are the second moment of area of the individual chord section and the overall built-up section, respectively, and L_G and L_B represent the length of a chord segment between lacing connectors and the total length of the built-up member, respectively.

$$N_{cr,G} = \frac{\pi^2 E I_{ch}}{L_G^2}, \text{ and } N_{cr,B} = \frac{\pi^2 E I}{L_B^2} \tag{7}$$

3. Numerical investigations

3.1 Key features and assumptions

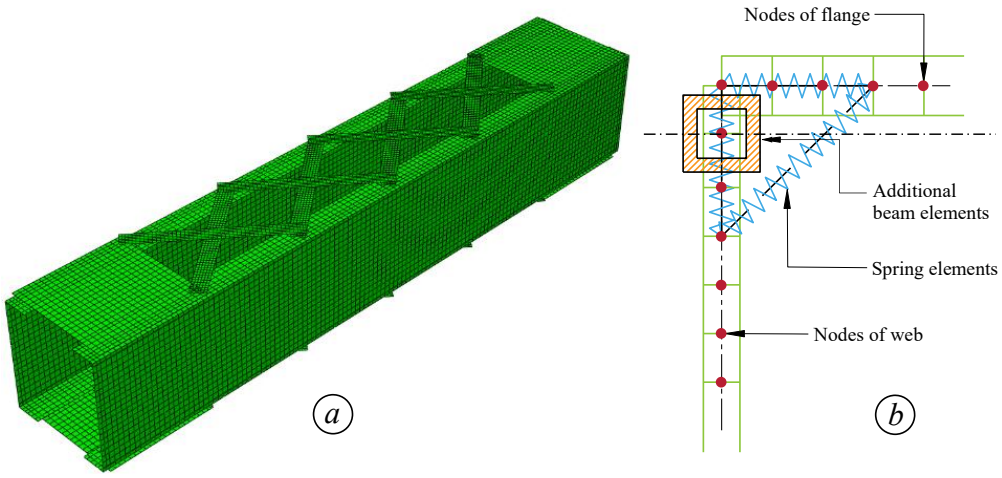

Figure 5: Numerical modeling – (a) Typical tip-to-tip arrangement with a double (X) lacing system – (b) Modeling of the area between the web and flange of chord members

Numerical models of laced built-up members were developed in the non-linear finite element software ABAQUS (Abaqus/CAE, 2022) to conduct parametric studies, with constraints applied to isolate specific buckling modes (Section 4). The built-up sections comprise two longitudinal chords arranged either tip-to-tip ([ ]) or back-to-back (] [), interconnected by flat X-shaped lacing bars and end tie-plates. All components were modeled using four-node shell elements (S4R), which have been widely validated in previous studies for their accuracy (Huang & Zhang, 2020; Wang et al., 2020; Li et al., 2022).

A mesh sensitivity study was carried out for geometrically and materially non-linear analyses with imperfections (GMNIA). Based on the results (Figure 5a), a mesh size equal to $1/20^{th}$ of the chord web depth was adopted, providing an efficient compromise between accuracy and computational cost. In addition, hollow beam sections and spring elements were introduced in the web-flange regions to represent fillet geometry, increase torsional rigidity and prevent local buckling within the fillet radius, following established approaches in the literature (Gagné et al., 2020; Gérard et al., 2021; Li et al., 2022) (Figure 5b).

3.2 Material characteristics and imperfections

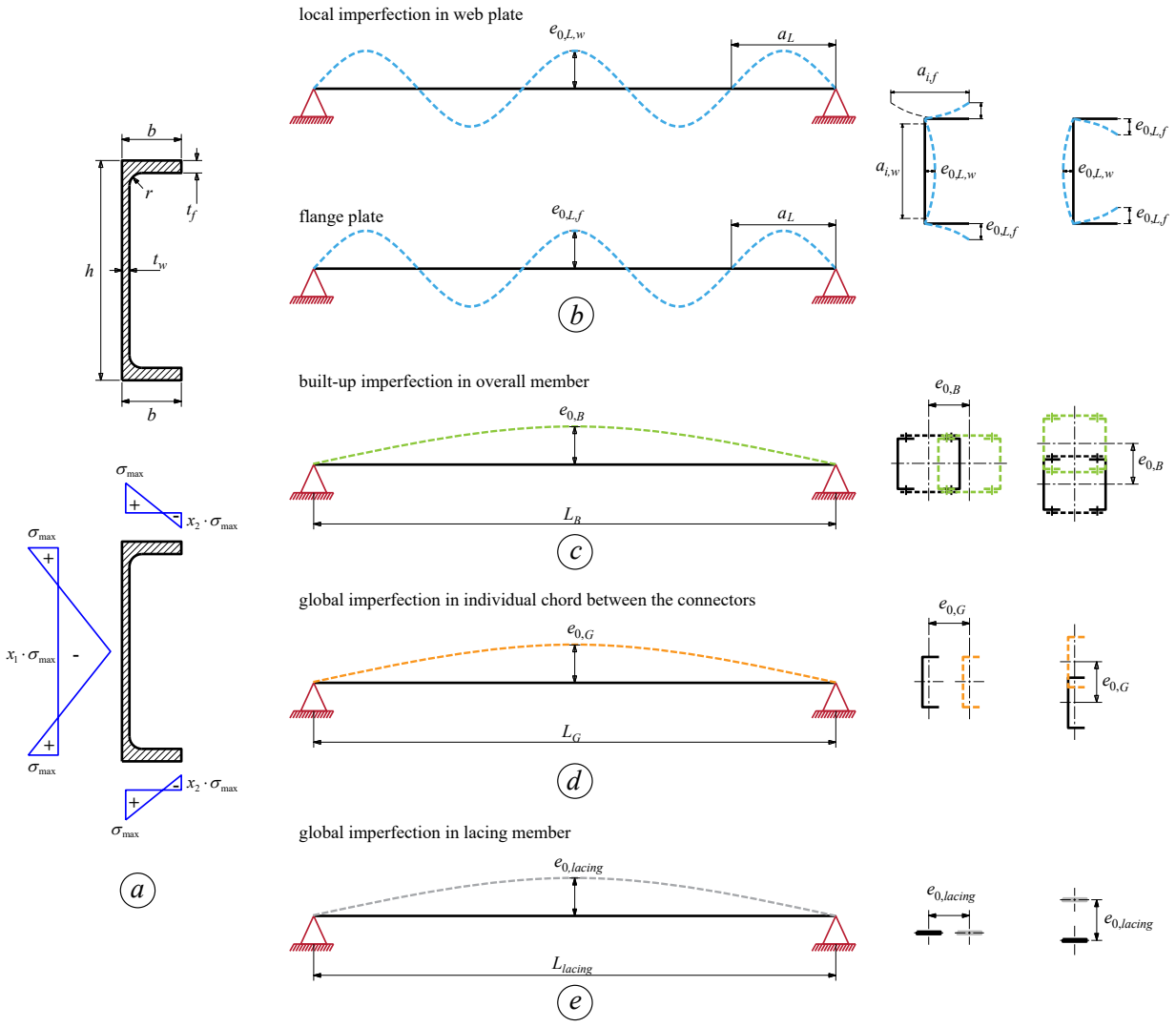

Figure 6: Definition of residual stresses and geometrical imperfections

The material behavior was modeled using a quad-linear stress-strain relationship (Yun & Gardner, 2017), converted into true stress and logarithmic plastic strain and implemented in ABAQUS for validation and parametric analyses. Residual stresses were introduced in the chords following the model proposed by Beyer et al. (2018) for C-sections. As shown in Figure 6a, the maximum residual stress is defined as $\sigma_{max} = 0.15\, f_y$, with factors $x_1 = 1 + b\, t_f / (h\, t_w)$ and $x_2 = 0.5$, where b and h are the section width and height, and t_w and t_f are the web and flange thicknesses. Local and global geometric imperfections were introduced by modifying shell node coordinates using sine-wave functions, following Eurocode recommendations (CEN, 2021; Johansson et al., 2007). As illustrated in Figure 6b, local imperfections were applied to the web and flange plates with half-wavelengths related to their flat widths, defined as $a_{i,w} = h - 2\,(t_f + r)$ and $a_{i,f} = 2\,(b - t_w - r)$. The corresponding amplitudes are denoted by $e_{0,L,w}$ and $e_{0,L,w}$. An odd number of half-waves was adopted to ensure the weakest cross-section occurs at mid-span (Mefande Wack et al., 2025). While Eurocode 3 typically applies global imperfections only to the overall member, this study

independently considers global imperfections for (i) the overall built-up member, (ii) individual chords between lacing connectors, and (iii) lacing members. This approach provides a more realistic representation and facilitates isolation of the buckling modes of each component for integration into the OIC framework. As shown in Figures 6c-6e, the corresponding half-wavelengths are defined as L_B, L_G and L_{lacing}, with amplitudes $e_{0,B}$, $e_{0,G}$, and $e_{0,lacing}$, respectively. All imperfections were applied along the minor bending axis and combined with residual stresses patterns. Further discussion is provided in Section 3.4.

3.3 Key features and assumptions

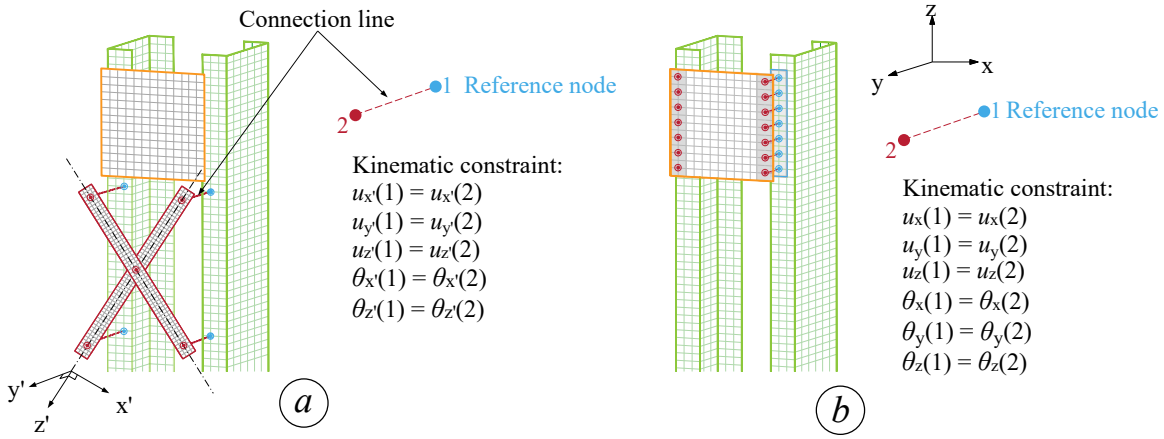

Figure 7: Connection modeling of – (a) lacing member to chord – (b) tie-plate to chord

In existing truss bridges with built-up members, connections between chords, lacing bars and tie-plates are typically riveted or bolted and are modeled using connection lines (Figure 7a). The lacing-to-chord joint is represented as a riveted connection allowing free in-plane rotation. This is achieved by applying a kinematic constraint between a reference node and a coupling node, enforcing identical translational and rotational degrees of freedom except for rotation about the rivet axis (y'), which remains free. This approach permits rotation about the y' axis while restraining other relative movements. End tie-plates are modeled similarly, but with all displacements and rotations fully constrained between connected nodes (Figure 7b). As shown in Figure 8, the built-up column is modeled under simply supported conditions, with translational constraints in the x and y directions and torsional rotation restrained at both ends ($u_x = u_y = \theta_z = 0$). The axial load is applied at a reference point at one end, while axial displacement is restrained at the opposite end. Reference points located at the cross-section centroid ensure uniform end displacements and can be offset by distances e_x and e_z to replicate experimental setups for numerical validation (Section 3.4).

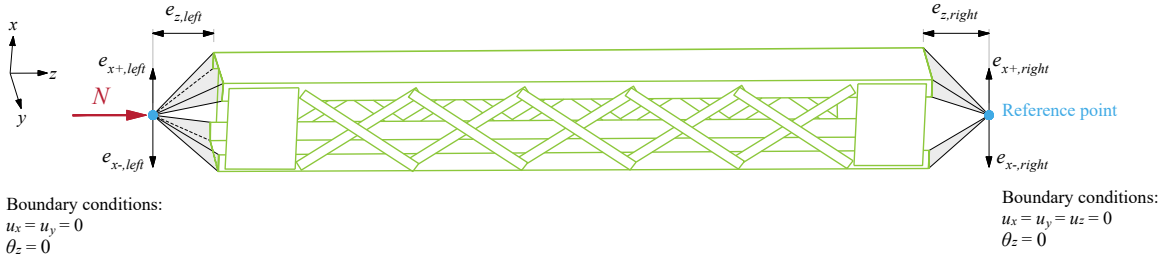

Figure 8: Boundary conditions of built-up members

3.4 Validation of numerical models

The finite element models were validated against experimental tests by Kleiser and Uang (1999), Lee and Bruneau (2008), Bonab et al. (2013), and Kalochairetis et al. (2014), covering 23 specimens with tip-to-tip and back-to-back built-up sections composed of C-shaped chords and lacing members. Most specimens were tested under static loading, while a few were subjected to cyclic loading; prior numerical studies (Chhoeng et al., 2025, 2026) showed that the difference between cyclic and static ultimate loads is below 2%. Consequently, all specimens were modeled under static loading. As summarized in Table 1, the columns were simply supported and subjected to concentric or eccentric compression, with some specimens restrained against mid-span out-of-plane displacement. Due to limited data on measured imperfections, a sensitivity study was conducted to determine appropriate amplitudes for local and global geometric imperfections of the cross-section, overall member, chords between connectors, and lacing members. Two imperfection combinations were examined: (i) local and overall global imperfections, $e_{0,L} + e_{0,B}$ (Case A), following Eurocode 3, and (ii) combined local, overall, chord and lacing imperfections, $e_{0,L} + e_{0,B} + e_{0,G} + e_{0,lacing}$ (Case B). Local imperfection amplitudes were defined as $e_{0,L} = a_L / 200$, consistent with Eurocode 3 and prior studies. For global imperfections, the overall member amplitude was set to 1 / 500 of the member length in Case A, while Case B additionally examined amplitudes of 1 / 500, 1 / 1000, and 1 / 1500.

$$e_{0,B} = \frac{L_B}{500} \tag{8}$$

$$\text{(i)} \quad e_{0,B} = \frac{L_B}{500}, \quad e_{0,G} = \frac{L_G}{500}, \quad e_{0,lacing} = \frac{L_{lacing}}{500}$$

$$\text{(ii)} \quad e_{0,B} = \frac{L_B}{1000}, \quad e_{0,G} = \frac{L_G}{1000}, \quad e_{0,lacing} = \frac{L_{lacing}}{1000} \tag{9}$$

$$\text{(iii)} \quad e_{0,B} = \frac{L_B}{1500}, \quad e_{0,G} = \frac{L_G}{1500}, \quad e_{0,lacing} = \frac{L_{lacing}}{1500}$$

Table 1 compares the ultimate load ratios $N_{u,FE} / N_{u,test}$ obtained from F.E. analyses and experiments. For Case A, which combines local and overall global imperfections (a_L / 200 and L / 500), the models show good agreement with tests, with an average ratio of 0.98 and a C.o.V. of 6.8%. As expected, reducing the global imperfection amplitude increases the predicted capacity. In Case B, which additionally includes global imperfections of the chord and lacing members, predictions become more conservative at the same global factor (1 / 500), with an average ratio of 0.94 and a C.o.V. of 7.0%. Conversely, using a factor of 1 / 1500 leads to unconservative predictions, while a factor of 1 / 1000 provides the best agreement, yielding an average ratio of about 0.99 and a C.o.V. of 6.6%.

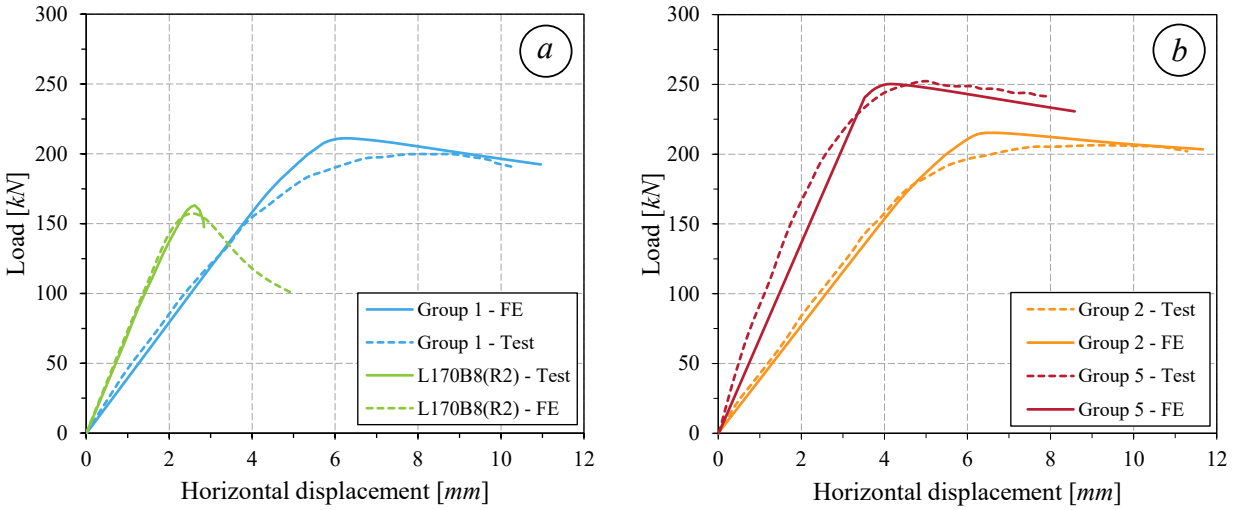

Figure 9: Load-displacement curves for – (a) specimens L170B8(R2) and Group 1 – (b) specimens Group 2 and Group 5, reported in (Bonab et al., 2013) and (Kalochairetis et al., 2014)

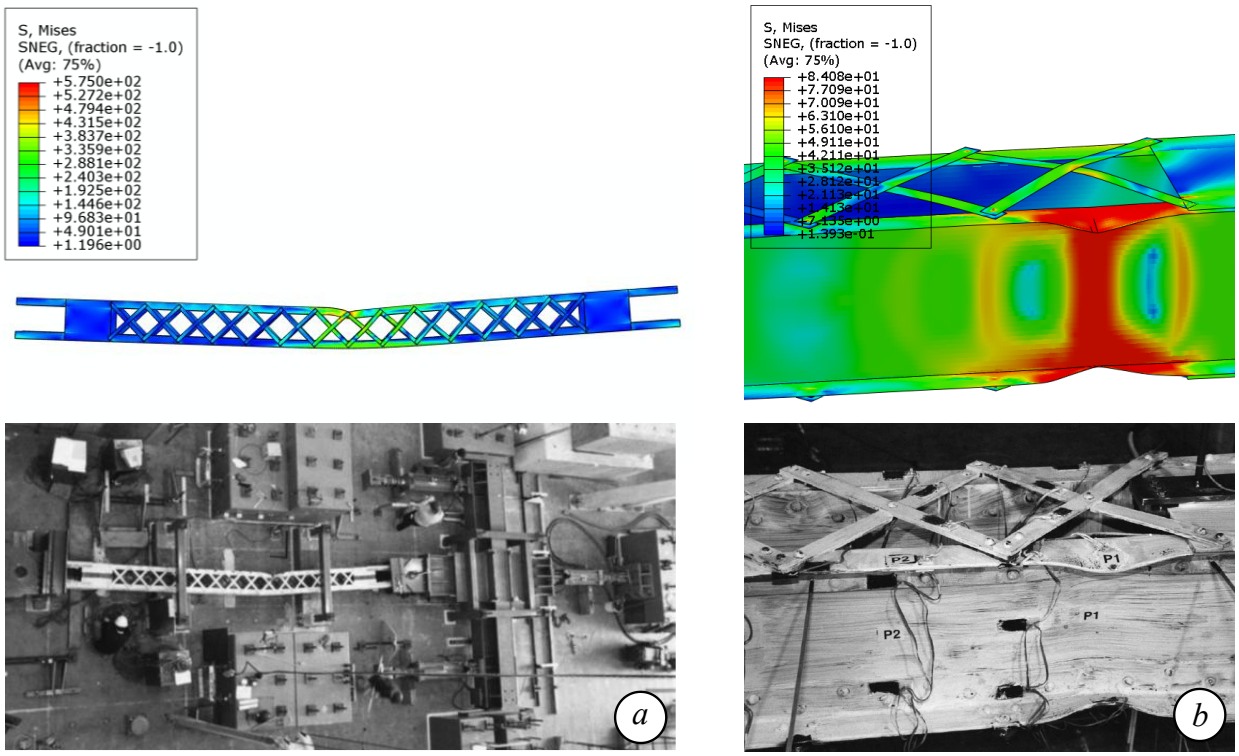

Figure 10: Comparison between F.E. and test failure modes for – (a) Specimen 3 – (b) Specimen 1 reported in (Kleiser & Uang, 1999) (stress is in *ksi*)

Figures 9 and 10 show that the F.E. models accurately reproduce the initial stiffness, ultimate strength, post-peak response and failure modes observed in experiments. The best correlation is achieved using the combined imperfection set $e_{0,L} = a_L / 200$, $e_{0,B} = L_B / 1000$, $e_{0,G} = L_G / 1000$, and $e_{0,lacing} = L_{lacing} / 1000$, which was therefore adopted for subsequent parametric studies. Under this configuration, the predicted strength ratios range from 0.88 to 1.11, confirming the reliability of the numerical models for further analyses.

Table 1: Summary of F.E. vs. test ultimate load of test specimens

References	Specimens	Loading positions				Ultimate loads and ratios				
		$e_{x,left}$ [mm]	$e_{z,left}$ [mm]	$e_{x,right}$ [mm]	$e_{z,right}$ [mm]	$N_{u,test}$ [kN]	$N_{u,FE}$ / $N_{u,test}$ [-] Global imperfection amplitude			
							Case A 1/500	Case B 1/500	Case B 1/1000	Case B 1/1500
Kleiser & Uang (1999)	Specimen 1	381	400	0	400	928.79	0.96	0.94	1.05	1.11
	Specimen 2	127	400	0	400	1633.83	1.01	0.97	0.95	1.01
	Specimen 3	0	400	0	400	2885.12	0.95	0.91	0.98	1.05
Lee & Bruneau (2008)	By8-120	0	0	0	0	295.81	0.95	0.90	0.94	0.99
	By16-60	0	0	0	0	521.64	0.91	0.87	0.93	0.99
	By16-120	0	0	0	0	447.00	0.98	0.92	0.95	1.18
	Bx8-60	0	0	0	0	267.16	1.05	1.01	1.11	1.17
	Bx8-120	0	0	0	0	213.51	1.11	1.04	1.07	1.15
	Bx16-60	0	0	0	0	506.87	1.09	0.99	1.01	1.09
	Bx16-120	0	0	0	0	409.50	1.02	0.98	1.10	1.17
Bonab et al. (2013)	L140B8(R1)	0	140	0	140	204.76	0.97	0.92	0.98	1.07
	L140B8(R2)	0	140	0	140	183.86	1.01	0.97	1.01	1.09
	L140B8(R3)	0	140	0	140	159.09	1.01	0.96	1.02	1.08
	L140B10(R1)	0	95	0	95	289.05	0.88	0.84	0.88	0.90
	L170B7(R1)	0	95	0	95	151.95	0.91	0.85	0.90	0.91
	L170B7(R2)	0	95	0	95	135.19	0.88	0.82	0.89	0.92
	L170B7(R3)	0	95	0	95	124.32	0.91	0.86	0.96	0.97
	L170B8(R2)	0	95	0	95	162.40	0.94	0.89	0.98	0.95
	L170B8(R3)	0	95	0	95	146.29	0.97	0.91	0.96	0.98
Kalochairetis et al. (2014)	Group 1	100	162.5	100	162.5	200.00	1.06	1.02	1.06	1.10
	Group 2	100	162.5	100	162.5	206.00	1.05	1.01	1.06	1.11
	Group 4	100	162.5	-80	162.5	230.00	1.07	1.04	1.07	1.13
	Group 5	50	162.5	50	162.5	247.00	1.01	0.98	1.01	1.07
						Mean	0.98	0.94	0.99	1.06
						C.o.V.	6.8 %	7.0 %	6.6 %	8.3 %
						Min.	0.88	0.82	0.88	0.90
						Max.	1.11	1.04	1.11	1.18

3.5 Parametric studies

Using the validated F.E. models, parametric studies were conducted to investigate the effects of chord arrangements, section dimensions, and member slenderness on the resistance of laced built-up columns. Each built-up section consisted of two hot-rolled C-shaped sections connected by double X-shaped lacing bars and end tie plates, arranged tip-to-tip or back-to-back, with rivet connections. All components were assumed to have steel grade CSA G40.4 ($f_y = 230\ MPa$), representative of Canadian structural steel from the 1950s, with minimal influence on buckling curve selection (Li et al., 2022). A total of 300 standard and invented C-shaped sections were studied to examine local, global and built-up behaviors, including L/G/B interaction. Invented sections were based on angle-connected C-shapes (Figure 1d), serving as equivalent references.

Section heights ranged from 152.5 *mm* to 1021 *mm* and widths from 30.5 *mm* to 152.4 *mm*, covering both non-slender and slender elements (web slenderness $h / t_w = 6$ to 96.95, flange slenderness $b / t_f = 4$ to 10.7. Lacing members were designed to remain elastic before the built-up member fails, with a minimum inclination of 25°. Overall, approximately 5 000 G.M.N.I.A. simulations were performed to determine ultimate loads and buckling reduction coefficients χ_L, χ_G, χ_B and χ_{L+G+B}.

4. Proposed O.I.C. design rules

4.1 Local, global, and built-up member buckling curves

Using the numerical results obtained from the parametric studies discussed in Section 3, the proposed design buckling curves for cross-section local behavior, global behavior of the chord between the connectors and built-up behavior of the overall member are presented in Figure 11 and Figure 12. Both figures plot the obtained results in "O.I.C. format", where the horizontal axis corresponds to the cross-section and members relative slenderness ($\bar{\lambda}_L$, $\bar{\lambda}_G$, and $\bar{\lambda}_B$) associated with the corresponding reduction factors χ_L, χ_G, and χ_B.

Local buckling:

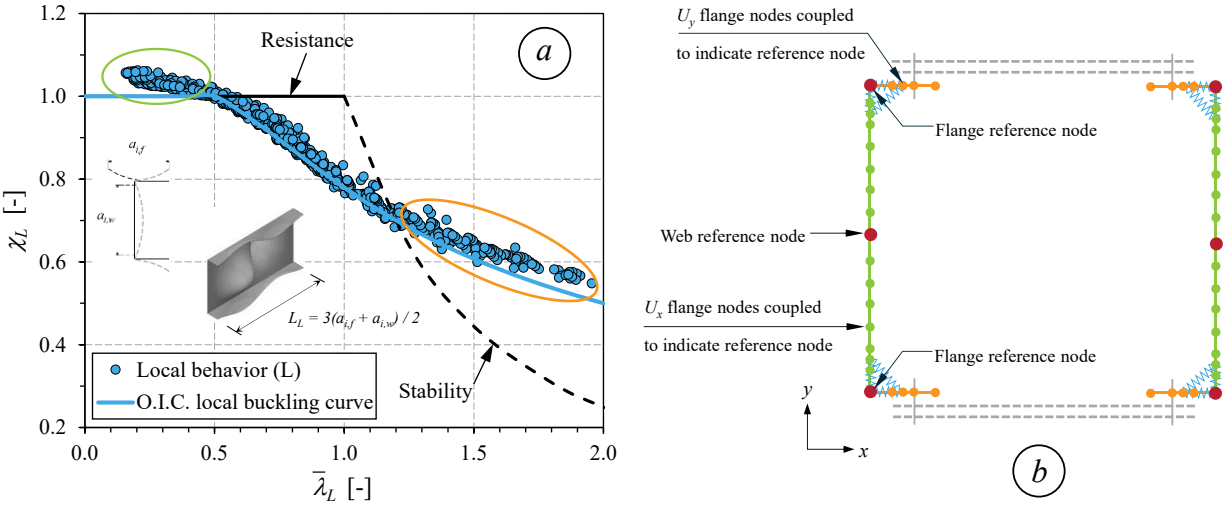

Figure 11: (a) O.I.C. buckling curve for cross-section resistance – (b) Plate buckling restraint

Figure 11a illustrates the *local buckling behavior* of the cross-section obtained from F.E. results in a $\chi_L - \bar{\lambda}_L$ format, along with two specific lines: (i) a horizontal solid line ($\chi_L = 1$), which indicates the plastic resistance, and (ii) a parabolic dashed line ($\chi_L = 1 / \bar{\lambda}_L^2$), which represents the limit elastic plate buckling where the design assumes an ideal plate free of imperfections. As can be seen, across all range of λ_L, values of the penalty factor χ_L differ by less than 5%, indicating that a single local buckling curve is sufficiently accurate and appropriate for use. Additionally, as indicated in the orange ellipse in Figure 11a, most slender C-shaped cross-sections experience post-buckling effects, resulting in a χ_L value exceeding the stability limit. Furthermore, most compact sections slightly exceed their plastic capacity due to the benefit of strain-hardening effects (see green ellipse).

Global buckling:

To isolate the *pure global buckling* behavior of a chord between connectors, a corresponding F.E. model was developed for a single chord with a total length of L_G, where L_G is the distance between lacing connections. To prevent local buckling in the cross-section and isolate global buckling, the vertical displacement (U_y) of each node along the flange plates was constrained to match the displacement of the reference node located at the corner of the section, while the horizontal displacement (U_x) of each node along the web plate was constrained to match the value of the reference node at the midpoint. Figure 11b illustrates the plate buckling constraint for a laced built-up member composed of two main chords. Note that in Figure 11b, a similar constraint is applied to isolate the global buckling of the chord between connectors, but only one chord is considered.

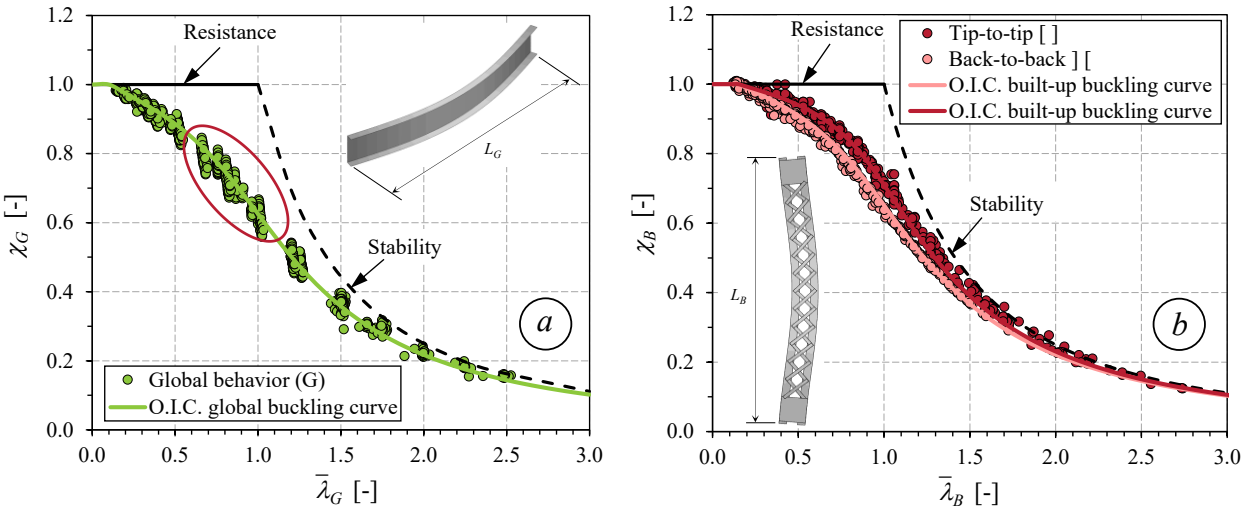

Figure 12: O.I.C. buckling curves for – (a) global buckling of chords between the connectors – (b) built-up buckling of the overall member

The proposed O.I.C. buckling curve for global buckling of the chord between the connectors is presented in Figure 12a. The F.E. data exhibits a slight dispersion, particularly for members with $\bar{\lambda}_G$ varying from 0.5 to 1.0, where the effects of geometrical imperfections and residual stresses are more pronounced. This is clearly illustrated by the red ellipse in Figure 12a, where the deviation, approximately 8%, arises from the varying section dimensions of the C-shaped profiles considered in this study. As expected, the resistance of long columns, specifically for $\bar{\lambda}_G > 1.5$ is primarily governed by global instability, with minimal influence from geometrical imperfections. This is evidenced by the fact that the results closely align with the "stability" limit line.

Built-up buckling:

Further, to ensure that only the *built-up buckling* of the overall member governs the behavior, the F.E. models were complemented with 2 additional constraints to prevent (i) local buckling of the cross-section, as indicated in Figure 11b, and (ii) global buckling of the chord between the connectors (i.e., not within the cross-section). This was achieved by limiting the spacing of the lacing connectors, L_G, so that the global slenderness $\bar{\lambda}_G$ remains close to the ideal slenderness $\bar{\lambda}_{G,0}$, ensuring that $\chi_G \approx 1$. This implies that the chord retains its full axial capacity, with no significant loss of strength due to buckling between connectors. The F.E. results for the built-up

buckling of the overall member are depicted in Figure 12b. Similarly, for built-up member resistance, the effects of residual stresses and imperfections are negligible in long members. Yet, clear trends can be observed for short and intermediate column lengths ($\overline{\lambda}_B < 1.5$) owing to different chord arrangements (tip-to-tip vs back-to-back). As illustrated in Figure 12b, the adoption of two separate buckling curves is therefore deemed fully appropriate, with an excellent level of consistency achieved, as indicated by the very limited scatter with respect to each curve.

The proposed O.I.C. design equations for local, global and built-up member buckling are presented in Table 2, in extension to the Ayrton-Perry format (Ayrton & Perry, 1886). Each equation addresses a distinct buckling mode (local, global or built-up), in order to evaluate their contributions separately, i.e., at this point, no coupling is accounted for. In accordance with this format, the proposed buckling curves for local buckling of the cross-section, global buckling of the chord between connectors and built-up buckling of the overall member are illustrated in Figure 11a, 12a, and 12b, respectively. These curves were precisely optimized by defining a set of key parameters: $\overline{\lambda}_0$, δ and α; $\overline{\lambda}_0$ relates to the length of the "plateau" where $\chi = 1.0$, δ considers any post-buckling strength and α is the generalized imperfection factor. For each buckling mode, α and $\overline{\lambda}_0$ are successively denoted as α_L, α_G and α_B, and $\overline{\lambda}_{0,L}$, $\overline{\lambda}_{0,G}$ and $\overline{\lambda}_{0,B}$; they lead to reduction factors χ_L, χ_G and χ_B relative to each buckling mode. As a particular point regarding built-up buckling in the plane of the lacing systems, the imperfection factor for the back-to-back section is greater than that of the tip-to-tip section, indicating that the proposed buckling curve for the back-to-back section is lower than that for the tip-to-tip section.

Table 2: Design procedure and key parameters for local, global, and built-up member buckling curves

Buckling resistance	Local buckling (L)	Global buckling (G)	Built-up buckling (B)
Key parameters	$\overline{\lambda}_{0,L} = 0.5$ $\alpha_L = 0.125$ $\delta_L = 0.7$	$\overline{\lambda}_{0,G} = 0.1$ $\alpha_G = 0.25$ $\delta_G = 2.0$	$\overline{\lambda}_{0,B} = 0.15$ $\alpha_B = \begin{cases} 0.14 \text{ for tip-to-tip sections} \\ 0.22 \text{ for back-to-back sections} \end{cases}$ $\delta_B = 2.0$
Reduction factor based on Ayrton-Perry format	$\phi_L = 0.5 \cdot \left[1 + \alpha_L \left(\overline{\lambda}_L - \overline{\lambda}_{0,L} \right) + \overline{\lambda}_L^{\delta} \right]$ $\chi_L = \frac{1}{\phi_L + \sqrt{\phi_L^2 - \overline{\lambda}_L^{\delta}}} \leq 1$	$\phi_G = 0.5 \cdot \left[1 + \alpha_G \left(\overline{\lambda}_G - \overline{\lambda}_{0,G} \right) + \overline{\lambda}_G^2 \right]$ $\chi_G = \frac{1}{\phi_G + \sqrt{\phi_G^2 - \overline{\lambda}_G^2}} \leq 1$	$\phi_B = 0.5 \cdot \left[1 + \alpha_B \left(\overline{\lambda}_B - \overline{\lambda}_{0,B} \right) + \overline{\lambda}_B^2 \right]$ $\chi_B = \frac{1}{\phi_B + \sqrt{\phi_B^2 - \overline{\lambda}_B^2}} \leq 1$

4.2 Interaction factor $f_{L/G/B}$

In Section 4.1, the cross-section reduction factor (χ_L) and the member buckling reduction factors (χ_G and χ_B) were derived independently, without considering possible interactions between local, global and built-up buckling. According to Eq. 5 and Figure 4, once local, global and built-up buckling have been characterized separately, their potential interactions are incorporated through a coupling factor $f_{L/G/B}$. In this respect, a stepwise approach was adopted. First, the interaction between global and built-up buckling modes was characterized by coupling factor $f_{G/B}$. Once this interaction is determined, the local buckling interaction with global-built-up response can be

incorporated by introducing an additional coupling factor $f_{L/GB}$. Values of $f_{G/B}$ and $f_{L/GB}$ can be obtained from the F.E. results of the parametric studies using Eq. 5, where χ_{G+B} is determined by applying constraints to prevent local buckling, while χ_{L+G+B} is obtained by relaxing all constraints. Their relationships with $\bar{\lambda}_B$ are depicted in Figure 13.

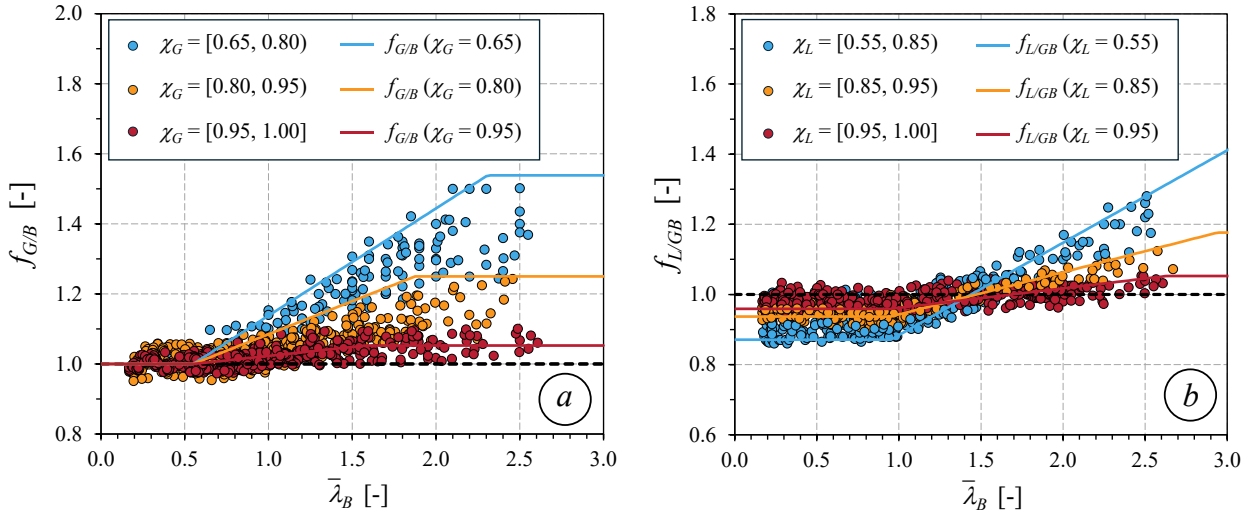

Figure 13: Interaction factors when considering – (a) Global/built-up interaction $f_{G/B}$ – (b) Local and global–built-up interaction $f_{L/GB}$

Overall, Figure 13 shows that $f_{G/B}$ and $f_{L/GB}$ vary with the overall slenderness of the built-up member $\bar{\lambda}_B$. Figure 13a illustrates the interaction results when considering global/built-up interaction. The scatter plot illustrates the relationship $f_{G/B} = \chi_{G+B} / (\chi_G \cdot \chi_B)$, assuming local buckling is ignored. Here, $f_{G/B}$ represents the influence of global buckling on built-up buckling (G/B interaction), where χ_{G+B} is the reduction factor accounting for the combined global and built-up buckling effects. The terms χ_G and χ_B denote the individual reduction factors from pure global buckling of chord between connectors and from built-up buckling, respectively. If $f_{G/B} < 1$, the interaction is adverse, meaning the combined effect reduces the strength more than expected. When $f_{G/B} \approx 1$, the two buckling mode act independently, so $\chi_{G+B} \approx \chi_G \cdot \chi_B$. If $f_{G/B} > 1$, the interaction is favorable, often occurring when global buckling of the chord between connectors has a minimal or negligible effect – leading to $f_{G/B} \approx 1/\chi_G$. From these cases, the interaction factor satisfies the condition $1 < f_{G/B} < 1/\chi_G$, defining the range where the interaction is favorable but less than the limiting case dominated solely by global buckling. Trilinear, conservative design equations for $f_{G/B}$ are given in Eq. 10, and their bounds are validated against numerical results in Figure 13a.

$$f_{G/B} = \begin{cases} 1 & \bar{\lambda}_B \le 0.55 \\ \dfrac{\bar{\lambda}_B - 0.55}{1.5/\chi_G - 0.55}\left(1/\chi_G - 1\right) + 1 & 0.55 < \bar{\lambda}_B \le 1.5/\chi_G \\ 1/\chi_G & \bar{\lambda}_B > 1.5/\chi_G \end{cases} \tag{10}$$

After defining the global/built-up interaction, the effect of local buckling can be considered by introducing an additional coupling factor, $f_{L/GB}$, which accounts for the influence of local buckling on the built-up behavior, the latter encompassing global buckling. The corresponding numerical results are presented in Figure 13b along with the proposed design equation for the $f_{L/GB}$ factor in Eq. 11.

$$f_{L/GB} = \begin{cases} k_L = 0.22 \cdot \chi_L + 0.75 & \bar{\lambda}_B \le 0.95 \\ \dfrac{\bar{\lambda}_B - 0.95}{2.5/\chi_L - 0.95}\left(1/\chi_L - k_L\right) + k_L & 0.95 < \bar{\lambda}_B \le 2.5/\chi_L \\ 1/\chi_L & \bar{\lambda}_B > 2.5/\chi_L \end{cases} \tag{11}$$

The function $f_{L/GB}$ is defined as a piecewise tri-linear interpolation with respect to the normalized relative slenderness $\bar{\lambda}_B$. For $\bar{\lambda}_B \le 0.95$, $f_{L/GB}$ remains constant at k_L, a factor that quantifies the adverse influence of local buckling on built-up behavior. In slender sections, where this effect is significant, k_L typically drops to around 0.75 and increases up to 0.97 as the section becomes stockier. Within the interval $0.95 < \bar{\lambda}_B \le 2.5/\chi_L$, the $f_{L/GB}$ transitions linearly from k_L to $1/\chi_L$, ensuring continuity and smoothness, and remains constant at $1/\chi_L$ for $\bar{\lambda}_B > 2.5/\chi_L$. In Figure 13b, it is revealed that for short columns ($\bar{\lambda}_B \le 0.55$), $f_{L/GB}$ remains below unity due to a significant impact of local buckling on the interactions. Similarly, for intermediate length columns ($\bar{\lambda}_B \le 0.95$), the built-up column is also affected by strong local interactions. This effect is more pronounced for built-up members with slender sections, i.e., sections with small χ_L values, where the interaction of local buckling results in relatively lower load-carrying capacities. Although $f_{L/G/B}$ continues to decrease as χ_L decreases, yet, in some cases, it tends to approach unity, particularly for compact sections where $\chi_L \approx 1$. This effect is accounted for by the coefficient k_L, as proposed in Eq. 11. Besides, it is noticed that the interaction effect of local buckling is less pronounced for built-up members with high relative slenderness ratios $\bar{\lambda}_B$. Therefore, for very long members, $f_{L/GB}$ is set to tend to $1/\chi_L$ in order to disregard the impact of local buckling. Additionally, the local interaction behavior should be accounted for intermediate length columns to fulfil the condition: $k_L < f_{L/GB} < 1/\chi_L$. As illustrated in Figure 13b, the proposed $f_{L/GB}$ expressions are compared to the F.E. results. It should be noted that each data point corresponds to their own $f_{L/GB}$ value. Here, only three upper bounds (safe) for $f_{L/GB}$ are presented. Once the $f_{G/B}$ and $f_{L/GB}$ factors are defined, the local/global/built-up interaction factor $f_{L/G/B}$ can be determined through Eq. 5, where $f_{L/G/B} = f_{G/B} \cdot f_{L/GB}$. It is observed that the proposed $f_{L/G/B}$ values are conservative and suitable for built-up members with various lacing spacings where the shear deformation is adequately accounted for. Besides, the suggested equations are safe and suitable for members with various slender sections and can be considered for short, intermediate and long columns. A more detailed discussion of the overall performance of the proposed design equations is presented in the next paragraph.

4.3 Assessment of design proposal

A comparison of numerical results, current design codes (AISC, AASHTO, Eurocode 3), and the proposed O.I.C. approach for laced built-up columns with double X-lacing is presented. Figure 14

shows performance for columns with two C-shaped sections in tip-to-tip ([ ]) and back-to-back (] [) arrangements, where each scatter point represents the capacity ratio for a specific member slenderness relative to a reference standard. Table 3 summarizes statistical measures (mean, C.o.V., min/max) and percentages of unconservative predictions exceeding 5%, 10%, and 15%, highlighting which design rules may underestimate member capacity. Significant overestimation (up to 10%) could compromise safety, with further reliability analysis discussed in Section 5.

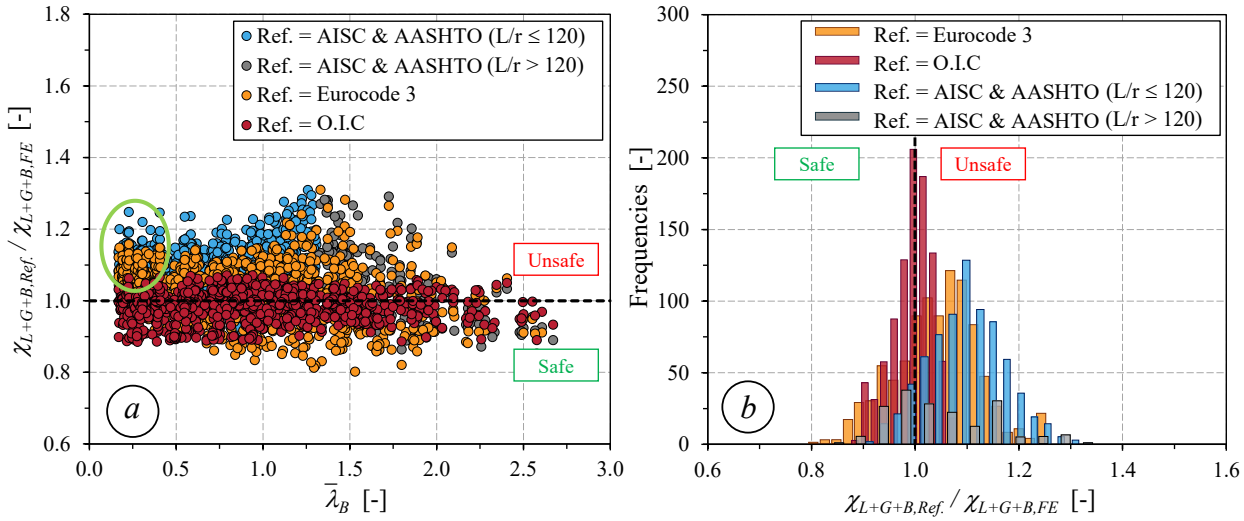

Figure 14: Analytical resistance predictions vs. numerical results

Overall, the main observation from Figure 14 and Table 3 indicate that the O.I.C.-based design rules can capture accurate resistance predictions, with an excellent mean $\chi_{L+G+B,\text{Ref.}} / \chi_{L+G+B,\text{FE}}$ value of 0.99 and a very low C.o.V. of 3.9%, while the worse result remains within 7% on the unsafe side. In turn, Eurocode 3 provides less accurate results compared to the proposed O.I.C. design equations, with a mean value of 1.05 and a C.o.V. of 7.5%. It is found that Eurocode 3 overestimates the average strength prediction by approximately 6% compared to the O.I.C. A more detailed analysis of the results highlights two key factors affecting its accuracy:

(i) The capacity of built-up members primarily relies on the resistance of the chord between the connectors, while only local buckling and global buckling are considered by Eurocode 3. However, even when the interaction between global and built-up buckling modes is minimal and local buckling governs the response ($\bar{\lambda}_B \approx \bar{\lambda}_0 \approx 0.14$), the maximum of the $\chi_{L+G+B,\text{Ref.}} / \chi_{L+G+B,\text{FE}}$ ratio still remains approximately 20% on the unsafe side (see green ellipse in Figure 14a). This suggests that the combined use of the effective area A_{eff} along with multiple global buckling curves, as currently prescribed in the code, may lead to inaccurate predictions;

(ii) Additionally, the code enforces a reduction in load due to the overall bending of built-up members but overlooks the interaction between local and global buckling coupled with built-up buckling behavior. This limitation is particularly evident in members with intermediate lengths ($\bar{\lambda}_B \approx 1.25$), where the worst case results in an overestimation of up to 31% on the unsafe side. Despite this, Eurocode 3 appears to be the safest standard, especially for intermediate ($\bar{\lambda}_B$ from 0.8 to 1.6) and long columns ($\bar{\lambda}_B > 1.6$), where about 11% and 18% of results fall below 0.9.

Table 3: Statistical results of $\chi_{L+G+B,Ref.} / \chi_{L+G+B,FE}$ ratio for all columns in this study

Relative slenderness	n	References	Mean	C.o.V. [%]	Max.	Min.	< 0.90 [%]	>1.05 [%]	>1.10 [%]	>1.15 [%]
$\bar{\lambda}_B \leq 0.8$	455	AISC & AASHTO ($L/r \leq 120$)	1.08	5.6	1.25	0.92	0.0	70.4	36.1	11.0
		Eurocode 3	1.03	5.3	1.16	0.86	1.1	43.4	10.1	0.2
		O.I.C.	0.98	4.1	1.07	0.89	5.6	2.7	0.0	0.0
$0.8 < \bar{\lambda}_B \leq 1.6$	399	AISC & AASHTO ($L/r \leq 120$)	1.10	8.5	1.31	0.91	0.0	70.3	48.8	29.7
		Eurocode 3	1.03	10.6	1.31	0.80	11.0	43.1	18.5	6.5
		O.I.C.	0.99	3.6	1.07	0.89	1.3	1.8	0.0	0.0
$\bar{\lambda}_B > 1.6$	108	AISC & AASHTO ($L/r > 120$)	1.04	9.7	1.29	0.85	5.6	22.2	12.0	5.6
		Eurocode 3	1.13	18.5	1.26	0.82	17.6	31.5	21.3	18.5
		O.I.C.	0.98	4.0	1.06	0.89	3.7	2.8	0.0	0.0
All $\bar{\lambda}_B$ values	952	AISC & AASHTO	1.09	7.5	1.31	0.85	0.6	65.6	40.7	19.7
		Eurocode 3	1.05	7.5	1.31	0.80	7.1	41.9	14.9	4.9
		O.I.C.	0.99	3.9	1.07	0.89	3.6	2.3	0.0	0.0

Further, AISC and AASHTO provisions exhibit quite worse results compared to Eurocode 3. Since AASHTO follows AISC recommendations for resistance predictions but imposes an additional constraint by limiting the slenderness ratio L/r to 120 for primary truss members, whereas AISC allows up to 200 for compression members, this restriction categorizes results into two sets: members that comply with the limit ($L/r \leq 120$) and those that exceed it ($L/r > 120$), which may not be acceptable under AASHTO provisions. It is observed that the overall results obtained from the American Standards are overly unconservative, with a mean $\chi_{L+G+B,\text{Ref.}} / \chi_{L+G+B,\text{FE}}$ ratio of 1.09 and a C.o.V. of 7.5% while the worse result reaching up to 31% on the unsafe side for members with $L/r \leq 120$. Yet, as reported in Table 3, approximately 66% of the results obtained from the American Standards, compared to the F.E. results, lie more than 5% on the unsafe side, whereas around 41% and 20% deviate up to 10% and 15% on the unsafe side, respectively. Furthermore, for members with $L/r > 120$, the American Standards also demonstrate a lack of consistency, with a mean $\chi_{L+G+B,\text{Ref.}} / \chi_{L+G+B,\text{FE}}$ ratio of 1.04 and a C.o.V. of 9.7%. Overall, in terms of lack of conservatism, the worst-case scenario reaches up to 31% on the unsafe side, with approximately 66%, 41%, and 20% of the data points remaining on the unsafe side at 5%, 10%, and 15%, respectively. In comparison, the O.I.C. approach provides excellent accuracy and better consistency, with a mean $\chi_{L+G+B,\text{OIC}} / \chi_{L+G+B,\text{FE}}$ ratio approximately equal to unity and a very low C.o.V. of around 4%. Besides, only 2.3% of the results exceed the 5% threshold on the unsafe side. Given the diverse member and section geometries considered, along with the complexity of local/global/built-up coupled instabilities analyzed in built-up members, the O.I.C. proposal proves to be a reliable design approach, ensuring accuracy, consistency, and safety.

5. Reliability analyses

Reliability analyses were carried out based on the recommendations of the First Order Reliability Method. Table 4 reports the results of the reliability analyses and the key statistical parameters considered, where n is the number of numerical and experimental results in each subset, $k_{d,n}$ is the design fractile factor, b is the mean value of the correction factor, $f_{y,mean} / f_{y,nom}$ is the material

overstrength factor and V_r is the combined coefficient of variation, which accounts for uncertainties from both the design model and the basic variables. The value of V_r was calculated using the following expression:

$$V_r^2 = V_\delta^2 + V_{rt}^2 \tag{12}$$

In Eq. 12, V_δ represents the C.o.V. of the uncertainties in the numerical and experimental resistance associated with the design models and $V_{r,t}$ is the C.o.V. of the uncertainties related to the k basic variables, where $V_{r,t}$ can be determined through Eq. 13 for each F.E. result, considering how the resistance depends on the variability of the two basic variables, i.e., geometry (V_{geom}) and material properties (V_{mat}).

$$V_{rt}^2 = V_{geom}^2 + V_{mat}^2 \tag{13}$$

In this study, statical data of material overstrength factor $f_{y,mean} / f_{y,nom}$ and the associated V_{mat}, along with V_{geom}, were adopted as recommended in Annex E of EN 1993-1-1. Finally, the mean partial safety factor required for the different cases considered was derived based on Eq. 14.

$$\gamma_M = \frac{1}{n}\sum_{i=1}^{n}\frac{r_{nom,i}}{r_{d,i}} \tag{14}$$

In Eq. 14, $r_{nom,i}$ is the nominal resistance calculated from F.E. models using the nominal values of material properties and $r_{d,i}$ is the design resistance determined as a function of the mean correction factor b and of the predicted resistance taken from the current standards and the O.I.C. proposal. More details about the calculation procedure can be found in (SAFEBRICTILE, 2016).

Table 4: Summary of reliability analysis results based on the Eurocode approach

Study cases	Proposals	n	$k_{d,n}$	b	$f_{y,mean} / f_{y,nom}$	V_{geom}	V_{mat}	V_δ	V_r	γ_M
Without T.A.	AISC & AASHTO	952	3.1	0.912	1.25	0.025	0.055	0.075	0.096	1.18
	Eurocode 3	952	3.1	0.953	1.25	0.025	0.055	0.075	0.097	1.13
	O.I.C.	952	3.1	0.986	1.25	0.025	0.055	0.040	0.072	1.01
With T.A.	AISC & AASHTO	701	3.104	0.888	1.25	0.025	0.055	0.052	0.080	1.15
	Eurocode 3	732	3.103	0.932	1.25	0.025	0.055	0.050	0.078	1.09
	O.I.C.	701	3.144	0.975	1.25	0.025	0.055	0.023	0.065	1.00

The Tail Approximation (T.A.) approach helps correct the excessive conservatism that results from incorrectly assuming normality for the full dataset, thereby improving the accuracy of safety and resistance factor calibration. As reported in Table 4, without adopting the T.A. technique, the γ_M value for the O.I.C. proposal was found to be an excellent 1.01, due to lower overall uncertainty – particularly attributed to the variability in geometry and material properties. In contrast, γ_M values associated with the American Standards and Eurocode 3 are 1.18 and 1.13, respectively. These values exceed the typical recommended limit – Eurocode 3 specifies a partial safety factor of $\gamma_M = 1.00$, which implies no safety margin for the cross-section and member. The Eurocode 3 value found here ($\gamma_M = 1.13$) reflects the need for a safety margin above 10%; AISC and AASHTO adopt a resistance factor $\phi = 0.90$, corresponding to $\gamma_M \approx 1 / \phi \approx 1.11$. A careful

analysis of these results indicates that these higher γ_M values primarily result from significant uncertainties in the design models, as reflected by a correction factor *b* lower than 1.0 and a higher V_δ. By applying the T.A. technique, γ_M factors for the American Standards and Eurocode 3 reduce to 1.16 and 1.10, respectively. This decrease is due to a drop in V_δ by disregarding the model uncertainty in the upper tail, thereby improving on previously conservative estimates of γ_M with more representative data. The O.I.C. method achieved a minimum γ_M of about 1.00, closely matching the actual resistance distribution. In conclusion, the O.I.C proposal shows more appropriate γ_M values compared to the other two proposals, suggesting it provides a more reliable design approach alongside superior accuracy, as discussed in previous paragraphs.

6. Conclusions

This paper investigated the buckling behavior of laced built-up columns subjected to pure compression loads, where buckling occurs within the plane of the lacing system. The built-up sections consisted of two main C-shaped sections interconnected by double (X) flat lacing bars. Results from extensive numerical analyses addressing local, global, and built-up buckling modes were presented. Non-linear shell F.E. models were carefully developed and validated against existing experimental results and subsequently used to conduct both preliminary and parametric studies. It was observed that laced built-up columns with slender elements are significantly influenced by cross-sectional local interactions and by complex local/global/built-up interaction modes. The original O.I.C.-based design approach was extended to address triple L/G/B interaction modes in laced built-up columns. This approach accounts for (i) local buckling of the cross-section of the chord, (ii) global buckling of the chord between lacing connectors, (iii) built-up buckling of the overall member and (iv) a local/global/built-up interaction factor $f_{L/G/B}$ to capture the interactions among the corresponding buckling modes. The performance and accuracy of the O.I.C. proposal, along with those of current design provisions, were evaluated against reference F.E. results. It was found that the American Standards and Eurocode 3 fail to adequately capture local/global/built-up interaction effects, leading to unconservative and scattered resistance predictions. In contrast, the O.I.C.-based design approach showed improved accuracy and consistency to the other design recommendations. Furthermore, reliability analyses incorporating the T.A. technique, conducted in accordance with EN 1990 framework, confirmed that the proposed O.I.C. design rules offer a safe and reliable method for designing laced built-up columns.

Acknowledgments

This research and development project would not have been possible without the contribution and collaboration of The Jacques Cartier and Champlain Bridges Incorporated.

References

A. Taras, V. Dehan, L. S. da Silva, L. Marques, T. Tankova. (2016). *SAFEBRICTILE: Standardization of Safety Assessment Procedures Across Brittle to Ductile Failure Modes*.

Abaqus/CAE (Version 2022). (2022). Dassault Systèmes. https://www.3ds.com/products-services/simulia/products/abaqus/

AISC. (2022). *Specification for Structural Steel Buildings*. ANSI/AISC 360-22, American Institute of Steel Construction, Chicago, IL.

American Association of State Highway and Transportation Officials (Ed.). (2020). *LRFD bridge design specifications* (9th edition). American Association of State Highway and Transportation Officials.

Anil Kumar, M. V., & Kalyanaraman, V. (2018). Interaction of Local, Distortional, and Global Buckling in CFS Lipped Channel Compression Members. *Journal of Structural Engineering*, *144*(2), 04017192. https://doi.org/10.1061/(ASCE)ST.1943-541X.0001935

AS 4100:2020. (n.d.). *Steel Structures, Standards Australia*.

Aslani, F., & Goel, S. (1991). An analytical criterion for buckling strength of built-up compression members. *Engineering Journal*, *28*, 159–168.

ATC. (1992). *Guidelines for Cyclic Seismic Testing of Components of Steel Structures* (No. ATC-24).

Ayrton, W. E., & Perry, J. (1886). On struts. *The Engineer*, *62*.

Basis of Design and Actions on Structures: Background and Application of Eurocode 1. (1996). *IABSE Colloquium*. IABSE Colloquium, Delft, The Netherlands.

Beyer, A., Boissonnade, N., Khelil, A., & Bureau, A. (2018). Influence of assumed geometric and material imperfections on the numerically determined ultimate resistance of hot-rolled U-shaped steel members. *Journal of Constructional Steel Research*, *147*, 103–115. https://doi.org/10.1016/j.jcsr.2018.03.021

Bleich, F. (1952). *Buckling Strength of Metal Structures*. McGraw-Hill.

Boissonnade, N., Hayeck, M., Saloumi, E., & Nseir, J. (2017). An Overall Interaction Concept for an alternative approach to steel members design. *Journal of Constructional Steel Research*, *135*, 199–212. https://doi.org/10.1016/j.jcsr.2017.02.030

Bonab, A. P., Hashemi, B. H., & Hosseini, M. (2013). Experimental evaluation of the elastic buckling and compressive capacity of laced columns. *Journal of Constructional Steel Research*, *86*, 66–73. https://doi.org/10.1016/j.jcsr.2013.03.014

Camotim, D., Martins, A. D., Dinis, P. B., Young, B., Chen, M.-T., & Landesmann, A. (2020). Mode interaction in cold-formed steel members: State-of-art report. *Steel Construction*, *13*(3), 186–207. https://doi.org/10.1002/stco.202000044

Cava, D., Camotim, D., Dinis, P. B., & Madeo, A. (2016). Numerical investigation and direct strength design of cold-formed steel lipped channel columns experiencing local–distortional–global interaction. *Thin-Walled Structures*, *105*, 231–247. https://doi.org/10.1016/j.tws.2016.03.025

CEN (European Committee for Standardization). (n.d.). *EN 1990:2002 Eurocode – Basis of Structural Design*.

CEN, European Committee for Standardization. (2021). *Eurocode 3: Design of Steel Structures – Part 1-14: Design Assisted by Finite Element Analysis* (prEN 1993-1-14:2020). European Committee for Standardization.

Chhoeng, O., Wack, M. C. M., Tremblay, R., & Boissonnade, N. (2025). *Stability and response of lacing systems in laced built-up truss bridge columns*. https://files.ssrcweb.org/proceedings/2025/Chhoeng_et_al_SSRC_2025.pdf

Chhoeng, O., Wack, M. C. M., Tremblay, R., & Boissonnade, N. (2026). Stability and design of built-up columns: Effect of 2nd order shear forces. *Journal of Constructional Steel Research*, *236*, 110052. https://doi.org/10.1016/j.jcsr.2025.110052

D. Beg, U. Kuhlmann, & L. Davaine. (2010). *ECCS Eurocode Design Manual: Design of Plated Structures*.

Dahboul, S., Coderre, T., Li, L., & Boissonnade, N. (2023). Behaviour and Design of I-Shaped Aluminium Sections. *Engineering Proceedings*, *43*(1), Article 1. https://doi.org/10.3390/engproc2023043035

Dahboul, S., Li, L., Coderre, T., & Boissonnade, N. (2023). O.I.C.-based design of extruded and welded aluminum I-sections. *Structures*, *58*, 105504. https://doi.org/10.1016/j.istruc.2023.105504

Dinis, P. B., Batista, E. M., Camotim, D., & dos Santos, E. S. (2012). Local–distortional–global interaction in lipped channel columns: Experimental results, numerical simulations and design considerations. *Thin-Walled Structures*, *61*, 2–13. https://doi.org/10.1016/j.tws.2012.04.012

Dinis, P. B., & Camotim, D. (2011). Local/distortional/global mode interaction in simply supported cold-formed steel lipped channel columns. *International Journal of Structural Stability and Dynamics*, *11*(05), 877–902. https://doi.org/10.1142/S0219455411004385

Dinis, P. B., Camotim, D., Batista, E., & Santos, E. (2011). Local / distortional / global mode coupling in fixed lipped channel columns: Behaviour and strength. *Advanced Steel Construction*, *7*(4), 113–130.

Dinis, P. B., Camotim, D., Young, B., & Batista, E. M. (2018). CFS lipped channel columns affected by L-D-G interaction. Part II: Numerical simulations and design considerations. *Computers & Structures*, *207*, 200–218. https://doi.org/10.1016/j.compstruc.2017.03.017

Duan, L., Reno, M., & Uang, C.-M. (2002). Effect of Compound Buckling on Compression Strength of Built-up Members. *Engineering Journal*, *39*, 30–37.

Engesser, F. (1891). Die Knickfestigkeit gerader Stäbe. *Centralblatt der Bauverwaltung*, *11*(49), 483.

European Committee for Standardization (CEN). (n.d.-a). *prEN 1993-1-1: Eurocode 3—Design of steel structures—Part 1-1: General rules and rules for buildings*.

European Committee for Standardization (CEN). (n.d.-b). *prEN 1993-1-5: Eurocode 3—Design of steel structures—Part 1-5: Plated structural elements*.

Gagné, A.-S., Gérard, L., & Boissonnade, N. (2020). Design of stainless steel cross-sections for simple load cases with the O.I.C. *Journal of Constructional Steel Research*, *168*, 105936. https://doi.org/10.1016/j.jcsr.2020.105936

Galbraith, & Holgate Derry. (1908). *Royal Commission on Quebec Bridge Inquiry*.

Gardner, L., Fieber, A., & Macorini, L. (2019). Formulae for Calculating Elastic Local Buckling Stresses of Full Structural Cross-sections. *Structures*, *17*, 2–20. https://doi.org/10.1016/j.istruc.2019.01.012

Gardner, L., Yun, X., & Walport, F. (2023). The Continuous Strength Method – Review and outlook. *Engineering Structures*, *275*, 114924. https://doi.org/10.1016/j.engstruct.2022.114924

Geng-Shu, T., & Shao-Fan, C. (1989). An interactive buckling theory for built-up beam-columns and its application to centrally compressed built-up members. *Journal of Constructional Steel Research*, *14*(3), 221–241. https://doi.org/10.1016/0143-974X(89)90074-6

Gérard, L., Li, L., Kettler, M., & Boissonnade, N. (2019). Recommendations on the geometrical imperfections definition for the resistance of I-sections. *Journal of Constructional Steel Research*, *162*, 105716. https://doi.org/10.1016/j.jcsr.2019.105716

Gérard, L., Li, L., Kettler, M., & Boissonnade, N. (2021). Steel I-sections resistance under compression or bending by the Overall Interaction Concept. *Journal of Constructional Steel Research*, *182*, 106644. https://doi.org/10.1016/j.jcsr.2021.106644

Handbook of Steel Construction (12th, 2nd Revised Printing ed.). (2023). Canadian Institute of Steel Construction.

Handbook of Structural Steelwork: Eurocode Edition. (2013). The British Constructional Steelwork Association Ltd and The Steel Construction Institute.

Huang, B., & Zhang, W. F. (2020). Local-overall interactive buckling of high strength steel welded I-section columns under axial compression. *Thin-Walled Structures*, *157*, 106964. https://doi.org/10.1016/j.tws.2020.106964

Johansson, B., Maquoi, R., Sedlacek, G., Müller, C., & Beg, D. (2007). *Commentary and Worked Examples to EN 1993-1-5 Plated Structural Elements*. https://publications.jrc.ec.europa.eu/repository/handle/JRC38239

Kalochairetis, K. E., Gantes, C. J., & Lignos, X. A. (2014). Experimental and numerical investigation of eccentrically loaded laced built-up steel columns. *Journal of Constructional Steel Research*, *101*, 66–81. https://doi.org/10.1016/j.jcsr.2014.04.032

Kleiser, M., & Uang, C.-M. (1999). Steel Latticed Members under Cyclic Axial and Flexural Actions. *Journal of Structural Engineering*, *125*(4), 393–400. https://doi.org/10.1061/(ASCE)0733-9445(1999)125:4(393)

Lee, K., & Bruneau, M. (2008). Seismic vulnerability evaluation of axially loaded steel built-up laced members I: Experimental results. *Earthquake Engineering and Engineering Vibration*, *7*(2), 113–124. https://doi.org/10.1007/s11803-008-0831-x

Li, L., & Boissonnade, N. (2022). Local/global coupled instabilities of slender I-sections under compression. *Thin-Walled Structures*, *172*, 108842. https://doi.org/10.1016/j.tws.2021.108842

Li, L., Dahboul, S., Verma, P., Dey, P., Fafard, M., & Boissonnade, N. (2023). O.I.C.-Based Design of Aluminum Circular Hollow Sections under Compression or Pure Bending. *Engineering Proceedings*, *43*(1), Article 1. https://doi.org/10.3390/engproc2023043031

Li, L., Fafard, M., & Boissonnade, N. (2022). Local and global instabilities of rolled T-section columns under axial compression. *Thin-Walled Structures*, *178*, 109517. https://doi.org/10.1016/j.tws.2022.109517

Li, L., Gérard, L., Kettler, M., & Boissonnade, N. (2022). The Overall Interaction Concept for the design of hot-rolled and welded I-sections under combined loading. *Thin-Walled Structures*, *172*, 108623. https://doi.org/10.1016/j.tws.2021.108623

Li, L., Gérard, L., Langlois, S., & Boissonnade, N. (2022). O.I.C.-based design of mono-symmetric I-sections under simple load cases. *Thin-Walled Structures*, *174*, 109134. https://doi.org/10.1016/j.tws.2022.109134

Li, Y., Cheng, W., Wang, B., & Ren, Y. (2019). Investigation on Elastic Compound Buckling of Latticed Columns Considering Eccentricity and Geometric Imperfections. *Advances in Mechanical Engineering*, *11*(5), 1687814019847400. https://doi.org/10.1177/1687814019847400

M. Kettler. (2008a). *Elastic-Plastic Cross-Sectional Resistance of Semi-Compact H- and Hollow Sections* [Ph.D. thesis]. Graz University of Technology.

M. Kettler. (2008b). *Elastic-Plastic Cross-Sectional Resistance of Semi-Compact H-and Hollow Sections*. Graz University of Technology.

Mefande Wack, M. C., Chhoeng, O., Tremblay, R., & Boissonnade, N. (2025). On the definition of geometric imperfections in the FE modelling of local buckling in hot-rolled channel sections. *Proceedings of the Annual Stability Conference Structural Stability Research Council, SSRC 2025*. https://publications.polymtl.ca/66106/

Michel, H. (2016). *Development of a New Design Method for Steel Hollow Section Members Resistance* [Ph.D. thesis]. University of Applied Sciences of Western Switzerland - Fribourg, University of Liège, Saint-Joseph University Beirut.

Nseir, J. (2015). *Development of a New Design Method for the Cross-Section Capacity of Steel Hollow Sections* [Ph.D. thesis]. University of Applied Sciences of Western Switzerland - Fribourg, University of Liège, Saint-Joseph University Beirut.

Ravindra, M. K., & Galambos, T. V. (1978). Load and Resistance Factor Design for Steel. *Journal of the Structural Division, ASCE*, *104*(ST9).

Rogers, C. A., & Hancock, G. J. (1996). *Ductility of G550 Sheet Steels in Tension—Elongation Measurements and Perforated Tests* (Research Report R735). University of Sydney.

SAFEBRICTILE. (2016). *Standardization of safety assessment procedures across brittle to ductile failure modes* (Guideline Deliverable D1.1; Grant Agreement Number: RFSR-CT-2013-00023). SAFEBRICTILE Project.

Santos, E. S., Batista, E. M., & Camotim, D. (2012). Experimental investigation concerning lipped channel columns undergoing local–distortional–global buckling mode interaction. *Thin-Walled Structures*, *54*, 19–34. https://doi.org/10.1016/j.tws.2012.02.004

Schafer, B. W. (2008). Review: The Direct Strength Method of cold-formed steel member design. *Journal of Constructional Steel Research*, *64*(7), 766–778. https://doi.org/10.1016/j.jcsr.2008.01.022

Seif, M., & Schafer, B. W. (2010). Local buckling of structural steel shapes. *Journal of Constructional Steel Research*, *66*(10), 1232–1247. https://doi.org/10.1016/j.jcsr.2010.03.015

Souza dos Santos, E., de Miranda Batista, E., & Camotim, D. (2014). Cold-formed steel columns under L-D-G interaction. *Steel Construction*, *7*(3), 193–198. https://doi.org/10.1002/stco.201410034

Steel Construction Manual (15th ed.). (2017). American Institute of Steel Construction (AISC).

Su, M. (2014). *Behaviour and design of aluminium alloy structural elements* (pp. 991039980209703414, b53280362) [Doctor of Philosophy, The University of Hong Kong]. https://doi.org/10.5353/th_b5328036

Svensson, S. E., & Kragerup, J. (1982). Collapse Loads of Laced Columns. *Journal of the Structural Division*, *108*(6), 1367–1384. https://doi.org/10.1061/JSDEAG.0005972

T. Usami, & Y. Fukumoto. (1984). Welded box compression members. *Journal of Structural Engineering (J. Struct. Eng.)*, *110*(10), 2457–2470.

Tankova, T., Simões da Silva, L., Marques, L., Rebelo, C., & Taras, A. (2014). Towards a standardized procedure for the safety assessment of stability design rules. *Journal of Constructional Steel Research*, *103*, 290–302. https://doi.org/10.1016/j.jcsr.2014.09.010

Timoshenko, S. P. (1930). Problems concerning elastic stability in structures. *Transactions of the American Society of Civil Engineers (Trans ASCE)*, *94*(1), 1000–1020.

Timoshenko, S. P., & Gere, J. M. (1961). *Theory of Elastic Stability*. Courier Corporation.

von Kármán, T., Sechler, E. E., & Donnell, L. H. (1932). The Strength of Thin Plates in Compression. *Transactions of the American Society of Mechanical Engineers*, *54*(2), 53–56. https://doi.org/10.1115/1.4021738

Wang, Y., Bradford, M. A., & Liu, X. (2020). Strength design of welded high-strength steel beams considering coupled local and global buckling. *Thin-Walled Structures*, *149*, 106391. https://doi.org/10.1016/j.tws.2019.106391

Young, B., Dinis, P. B., & Camotim, D. (2018). CFS lipped channel columns affected by L-D-G interaction. Part I: Experimental investigation. *Computers & Structures*, *207*, 219–232. https://doi.org/10.1016/j.compstruc.2017.03.016

Young, B., & Rasmussen, K. J. R. (1999). *Behaviour of cold-formed singly symmetric columns*. http://hub.hku.hk/handle/10722/150128

Young, B., & Yan, J. (2002). Channel Columns Undergoing Local, Distortional, and Overall Buckling. *Journal of Structural Engineering*, *128*(6), 728–736. https://doi.org/10.1061/(ASCE)0733-9445(2002)128:6(728)

Yun, X., & Gardner, L. (2017). Stress-strain curves for hot-rolled steels. *Journal of Constructional Steel Research*, *133*, 36–46. https://doi.org/10.1016/j.jcsr.2017.01.024